NASA TECHNICAL NOTE

NASA TN D-5244

c. 1

NASA TN D-5244

CIRCULATING CURRENTS IN LINEAR CROSSED-FIELD GENERATORS AND ACCELERATORS

by Gustav A. Carlson

Ames Research Center

Moffett Field, Calif.

NATIONAL AERONAUTICS AND SPACE ADMINISTRATION • WASHINGTON, D. C. • MAY 1969

CIRCULATING CURRENTS IN LINEAR CROSSED-FIELD GENERATORS AND ACCELERATORS

By Gustav A. Carlson

Ames Research Center
Moffett Field, Calif.

NATIONAL AERONAUTICS AND SPACE ADMINISTRATION

For sale by the Clearinghouse for Federal Scientific and Technical Information
Springfield, Virginia 22151 – CFSTI price $3.00

CIRCULATING CURRENTS IN LINEAR CROSSED-FIELD GENERATORS AND ACCELERATORS

By Gustav A. Carlson

Ames Research Center

SUMMARY

Boundary layers on the walls of linear crossed-field plasma generators and accelerators cause circulating electrical currents that can greatly affect the operation of these devices. Expressions are derived for the velocity and current distributions in the open circuit device from the analysis for fully developed incompressible magnetohydrodynamic (MHD) flow in a square duct with nonconducting walls. From these distributions the viscous and ohmic heat generation rates in the working fluid were calculated for Hartmann numbers up to 24, where the magnetic force is dominant. Measured heat-transfer rates to the walls of an open circuit J × B plasma accelerator were found to increase with applied magnetic field strength at the insulator walls but to remain nearly constant at the electrode walls. A comparison of theory and experiment indicates that the calculated heat generation has both the magnitude and spatial distribution to explain the observed heat-transfer rates. The circulating currents significantly decelerate the flow near the center of the duct, and will exist in any MHD duct in which there is an appreciable boundary layer and a large conductivity extending to near the walls.

INTRODUCTION

In most cases the simple one-dimensional theory of magnetohydrodynamic duct flow overpredicts the actual performance of linear crossed-field plasma generators and accelerators. Most attempts to extend the theory so it will better predict actual performance have been directed toward the description of the current distribution in the plane perpendicular to the applied magnetic field. Factors which influence the current distribution in that plane include electrode segmentation, velocity and thermal boundary layers on cold electrodes, Hall effects, unequal electron and gas temperatures, and nonequilibrium ionization. These factors have been shown to prevent the desired axial orientation of the J × B force (refs. 1-5). For open circuit operation of a J × B device, these investigations predict that the only magnetic effect will be an induced voltage proportional to the product of the applied magnetic field and the fluid velocity. Experimental measurements have departed from this prediction: The induced open circuit voltage is less than calculated from theory (refs. 6, 7); the impact pressure decreases with increasing magnetic field; and the heat transfer to the insulator walls is greater than that estimated for ordinary boundary layers (ref. 8).

This degradation of performance is caused by electrical currents which circulate within the working fluid. Circulating current loops in a linear J × B device may extend in the axial direction (end looping), or may lie in the plane perpendicular to the direction of flow. End looping (refs. 9, 10) is caused by axial variations in the applied magnetic field and will not be treated in this paper. Circulating currents in the plane perpendicular to the direction of flow are caused by the nonuniform axial velocity distribution. Schneider and Wilhelm (ref. 7) utilize the well known Hartmann problem to show qualitatively how these circulating currents can cause induced open circuit voltage to have a nonlinear dependence on magnetic field. Reilly and Oates (ref. 8) discuss these circulating currents as a source of ohmic heating and as the cause of increased shear at the insulator walls; however, they report experimental measurements of local heat transfer for only one value of magnetic field and present no calculations for boundary-layer heat transfer that include the effects of the circulating currents.

The purposes of this paper are (1) to report the results of calculations of the heat generation in the working fluid of an open circuit J × B device that include the effects of the circulating currents, and (2) to compare these calculations to experimental measurements of bulk heat transfer to the duct walls for various values of applied magnetic field. It must be noted that the calculations are for heat generation, whereas the measurements are for heat transfer, and that an increase in heat generation exceeds the corresponding increase in heat transfer by the amount of thermal energy increase of the fluid.

SYMBOLS

a	half-width of square duct
$\bar{B}$	magnetic induction vector
B_o	applied magnetic induction
$\bar{E}$	electric field strength vector
$\bar{H}$	magnetic field strength vector
H	Hartmann number, $B_o a \sqrt{\frac{\sigma}{\mu}}$
H_x	axial component of magnetic field strength
$\bar{J}$	current density vector
j_y	current density in y direction
j_z	current density in z direction
l	duct length

p	static pressure
q_j	rate of ohmic heat generation per unit volume
q_v	rate of viscous heat generation per unit volume
Q	rate of heat generation or heat transfer
$\bar{U}$	velocity vector
u	axial velocity
$\hat{u}$	average axial velocity
x,y,z	Cartesian coordinates
y^*	dimensionless coordinate, $\frac{y}{a}$
z^*	dimensionless coordinate, $\frac{z}{a}$
μ	dynamic viscosity of fluid
ρ	density of fluid
σ	electrical conductivity of fluid
$( )^*$	dimensionless quantity

THEORETICAL ANALYSIS

The duct configuration and coordinate system for the circulating current model are shown in figure 1. In this model the applied magnetic field B_o is assumed constant with only a z component. The axial velocity of the electrically conducting working fluid varies in both the y and z directions because of the boundary layers on the walls of the duct. This variation results in a nonzero value for curl $(\bar{U} \times \bar{B})$; however, Maxwell's electric field equation requires curl $(\bar{E}) = 0$. It follows from Ohm's law, $\bar{J} = \sigma(\bar{E} + \bar{U} \times \bar{B})$, that $\bar{J}$ is not zero, even for the open circuit case.

The circulating currents in the y-z plane of the open circuit duct are calculated from the analysis for fully developed incompressible MHD flow in a rectangular duct with nonconducting walls. The circulating current loops are assumed to remain entirely within the fluid as shown in figure 1. Such a current loop is more likely than one that includes current flow through the electrodes in the z direction (as assumed in the Hartmann problem) because the electrode-plasma interface resistance is appreciable. The nonconducting wall problem was solved exactly by Shercliff (ref. 11) in 1953 and has since been considered by others. For this paper, the exact solution presented by Hughes and Young (ref. 12) is the most useful.

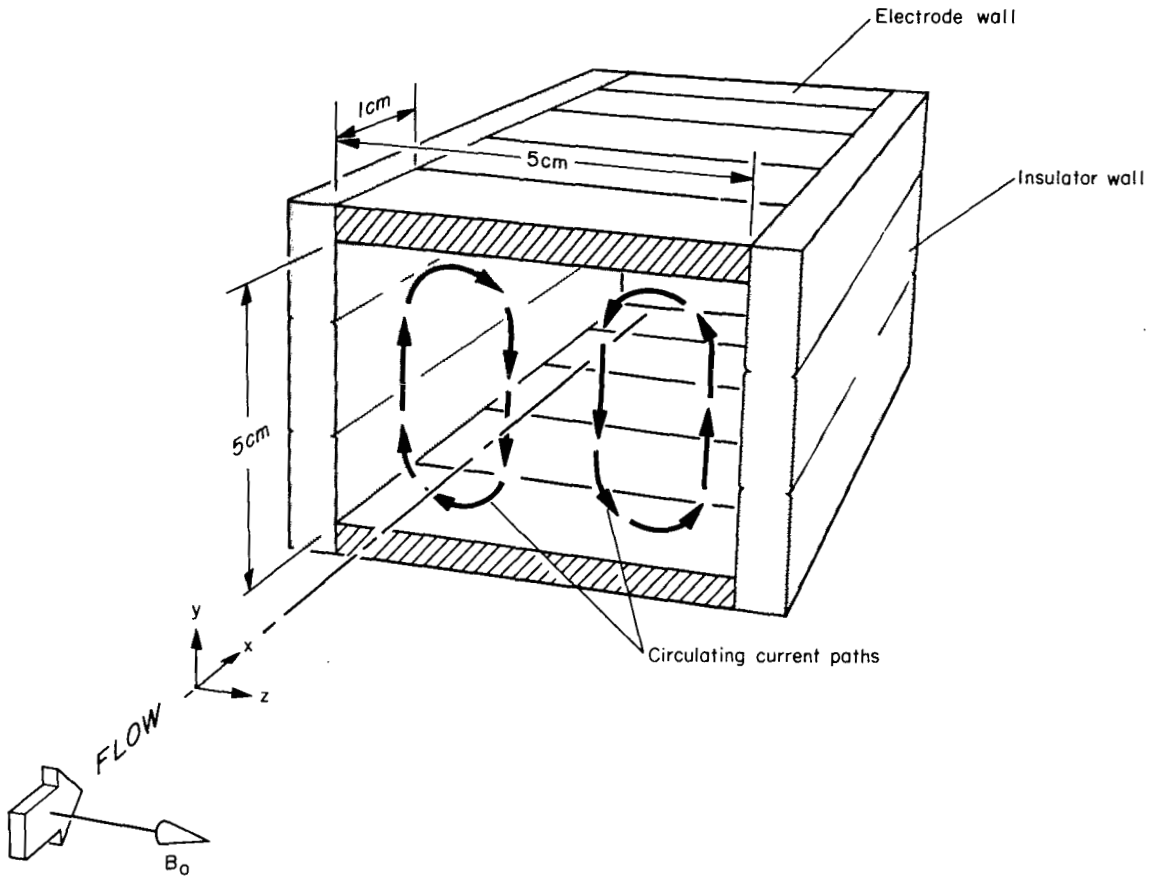

Figure 1.- The MHD duct.

Hughes and Young write the Navier-Stokes equation for fully developed, incompressible steady flow and combine the Maxwell equations $\nabla \times \bar{E} = 0$ and $\nabla \times \bar{H} = \bar{J}$ with Ohm's law for constant conductivity $\bar{J} = \sigma(\bar{E} + \bar{U} \times \bar{B})$ to form the steady-state magnetic transport equation. For the coordinate system of figure 1 the two final equations are

$$\mu\left(\frac{\partial^2 u}{\partial y^2} + \frac{\partial^2 u}{\partial z^2}\right) - B_o \frac{\partial H_x}{\partial z} - \frac{dp}{dx} = 0 \tag{1}$$

and

$$\frac{\partial^2 H_x}{\partial y^2} + \frac{\partial^2 H_x}{\partial z^2} + \sigma B_o \frac{\partial u}{\partial z} = 0 \tag{2}$$

For flow in a rectangular duct with nonconducting walls, Hughes and Young show that the solution to equations (1) and (2) may be expressed as simple Fourier series. The dimensionless form of their solution is not well suited for calculations of magnetic effect with flow rate held constant. With a choice of

dimensionless parameters better suited for such calculations, their solution for velocity, current, and pressure gradient in a square duct becomes

$$u^* = \frac{u}{\hat{u}} = \frac{1}{C}\left\{\frac{1-y^{*2}}{2} - 2\sum_{n=0}^{\infty} \frac{(-1)^n \cos \lambda_n y^* \left[-P_1\left(\lambda_n^2 - P_2^2\right) \frac{\tanh P_2}{\tanh P_1} \frac{\cosh P_1 z^*}{\cosh P_1} + P_2\left(\lambda_n^2 - P_1^2\right) \frac{\cosh P_2 z^*}{\cosh P_2}\right]}{\lambda_n^3 A_n}\right\} \tag{3}$$

$$j_y^* = \frac{j_y a}{\hat{u}\sqrt{\sigma\mu}} = \frac{1}{C}\left[2H\sum_{n=0}^{\infty} \frac{(-1)^n \cos \lambda_n y^* \left(-P_1 \frac{\tanh P_2}{\tanh P_1} \frac{\cosh P_1 z^*}{\cosh P_1} + P_2 \frac{\cosh P_2 z^*}{\cosh P_2}\right)}{\lambda_n A_n}\right] \tag{4}$$

$$j_z^* = \frac{j_z a}{\hat{u}\sqrt{\sigma\mu}} = \frac{1}{C}\left[2H\sum_{n=0}^{\infty} \frac{(-1)^n \sin \lambda_n y^* \left(-\frac{\sinh P_1 z^*}{\sinh P_1} + \frac{\sinh P_2 z^*}{\sinh P_2}\right)}{A_n}\right] \tag{5}$$

and

$$\left(\frac{dp}{dx}\right)^* = \frac{dp}{dx}\frac{a^2}{\hat{u}\mu} = -\frac{1}{c} \tag{6}$$

where

$$c = \frac{1}{3} + 4H\sum_{n=0}^{\infty} \frac{\sqrt{\lambda_n^2 + (H^2/4)}\,\tanh p_2}{\lambda_n^4 A_n}$$

$$A_n = -H\lambda_n^2\left(\frac{\tanh p_2}{\tanh p_1} + 1\right)$$

$$p_{1,2} = \sqrt{\lambda_n^2 + (H^2/4)} \pm H/2$$

$$\lambda_n = \frac{2n+1}{2}\Pi$$

The local heat generation rate in the flow is divided into two parts, the viscous term $q_v = \mu[(\partial u/\partial y)^2 + (\partial u/\partial z)^2]$ and the ohmic term $q_j = (1/\sigma)(j_y^2 + j_z^2)$. These terms are calculated in dimensionless form from equations (3) through (5) assuming both σ and μ constant:

$$q_v^* = q_v\left(\frac{a^2}{\hat{u}^2\mu}\right) = \left(\frac{\partial u^*}{\partial y^*}\right)^2 + \left(\frac{\partial u^*}{\partial z^*}\right)^2 \tag{7}$$

$$q_j^* = q_j\left(\frac{a^2}{\hat{u}^2\mu}\right) = (j_y^*)^2 + (j_z^*)^2 \tag{8}$$

The total heat generation rates are found by integrating equations (7) and (8) over the volume of the duct. Applying Green's theorem and substituting from equations (1) and (2) simplifies the integration to yield the following solution for total viscous and ohmic heat generation:

$$Q_v^* = \frac{Q_v}{4\hat{u}^2\mu l} = -\left(\frac{dp}{dx}\right)^* - H\int_0^1\int_0^1 u^* j_y^*\, dy^*\, dz^* \tag{9}$$

$$Q_j^* = \frac{Q_j}{4\hat{u}^2\mu l} = H\int_0^1\int_0^1 u^* j_y^*\, dy^*\, dz^* \tag{10}$$

The integral in equations (9) and (10) is evaluated numerically by a double application of Simpson's rule. The total heat generation rate (viscous plus ohmic) may be calculated without numerical integration, since the sum of equations (9) and (10) is simply

$$Q_{TOT}^* = \frac{Q_{TOT}}{4\hat{u}^2\mu l} = -\left(\frac{dp}{dx}\right)^* \tag{11}$$

The calculations for local and total heat generation rates were carried out for 11 values of Hartmann number, from 0.5 where the magnetic body force is negligible to 24 where it is dominant.

EXPERIMENT

The experiment was conducted on a linear J × B accelerator depicted schematically in figure 1. The accelerator channel is square at the entrance and diverges at a 2° half-angle in the x-y plane. There are 22 pairs of copper electrodes separated in the flow direction by 0.07-cm air gaps. The insulator walls are constructed of anodized aluminum and are insulated from the electrodes. As a further safeguard against shorting, each insulator wall of the channel consists of three slabs, with segmentation in the y direction. The electrodes and insulator walls are water cooled. The accelerator exhausts into a vacuum tank (operating pressure 2.5 mm Hg) and is fed by a supersonic constricted-arc jet (ref. 13) 1.27 cm in diameter and 30 cm long. The working fluid is unseeded argon added at the upstream end of the arc jet at a rate of 3.65 g/s. The steady-state arc jet operating conditions are 600 A dc at 400 V. In the work reported here the accelerator was operated in the open circuit condition with values of applied magnetic field from 0 to 0.5 tesla (T).

During each run a pitot probe and a stagnation heat-transfer rate probe were traversed in the y direction through the center of the plasma stream just downstream of the accelerator exit. Data from these probes were used to calculate the centerline velocity of the flow (refs. 14, 15). The velocity was independently checked by time of flight measurements of luminosity perturbations at the centerline of the plasma.

The heat-transfer rate to each of the accelerator walls was recorded continuously by a galvanometer-type oscillograph. This was accomplished by delta-T transducers (ref. 16) which measured the temperature rise of the water in each coolant circuit (see fig. 2). The pressure drop through each coolant circuit was maintained constant from run to run, thus insuring an invariant flow rate. The calibration constants for the transducer-oscillograph system were obtained directly from known amounts of electrical power dissipated in sections of high electrical resistance tubing that form a permanent part of each coolant circuit.

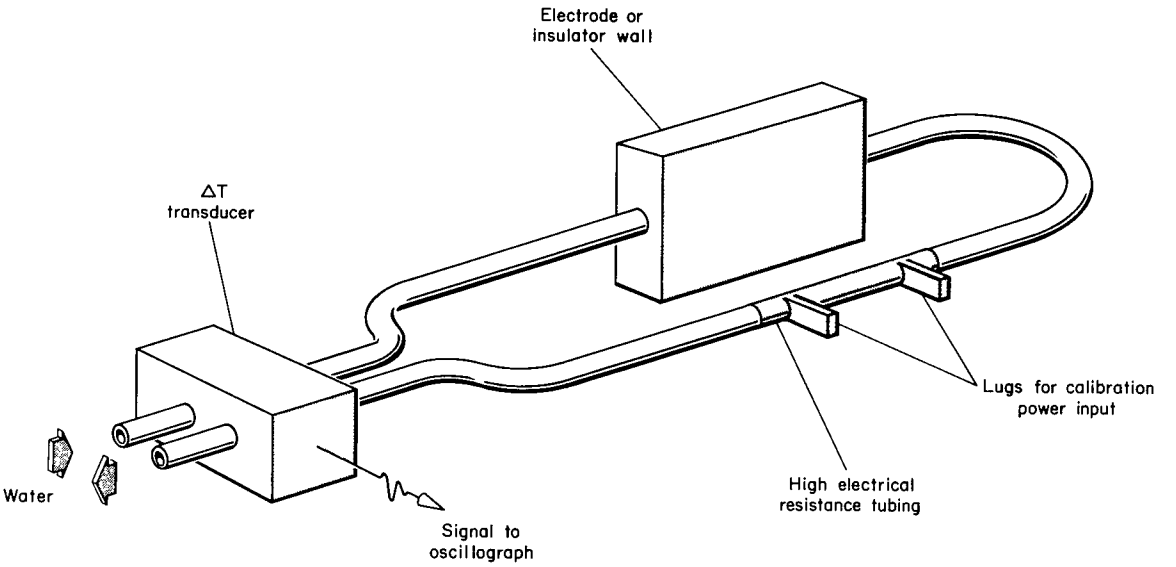

Figure 2.- Typical coolant circuit.

The measured wall heat-transfer rates were made dimensionless functions of the Hartmann number by use of the duct dimensions, a dynamic viscosity of 2×10^{-4} N·s/m^2, an electrical conductivity of 700 mho/m, and an average velocity of 2750 m/s.

$$Q^* = \frac{Q}{4\hat{u}^2 \mu l} \tag{12}$$

$$H = B_o a\sqrt{\sigma/\mu} \tag{13}$$

The transport properties were taken from De Voto (ref. 17) for equilibrium argon at 10 mm Hg pressure and 8000° K temperature, the approximate operating conditions in the accelerator. From the velocity relation for fully developed

flow in a square duct, $u(y = z = 0) \approx 2.1\ \hat{u}$, the average velocity was estimated as half the measured centerline velocity at zero magnetic field conditions. The fully developed flow relation was used because the traversing pitot probe measured a parabolic impact pressure profile, indicating that the wall boundary layers filled the duct. Although the quantitative comparison of experiment and theory is only as good as the estimates for viscosity, conductivity, and average velocity, the qualitative comments which follow are not dependent on these estimates.

COMPARISON OF THEORY AND EXPERIMENT

The spatial distributions of the calculated ohmic and viscous heat generation rates for Hartmann numbers of 1 and 10 are shown in figures 3 and 4. At the smaller Hartmann number, the viscous heat generation distribution is nearly symmetric about the duct diagonal, and the ohmic generation is very small. At the larger Hartmann number, both the viscous and the ohmic heat generation are much increased. (Note the change of scale between figs. 3 and 4.) These increases are caused by large circulating currents which develop as the Hartmann number is increased, with the largest current density appearing adjacent to the insulator walls. These currents result in correspondingly large ohmic heat generation and, in addition, cause a flattening of the velocity distribution in the z direction, which increases viscous heat generation because of the increased velocity gradient at the wall.

The measured values of heat transfer at $H = 0$ were 6.79 kW to the insulator walls and 2.33 kW to each of the electrode walls. As H was increased to 23, the measured heat transfer to the insulator walls increased to 25.2 kW, but the heat to the electrodes remained nearly constant. This concentration on the insulator walls of the heat-transfer increase with H is in excellent qualitative agreement with the calculated heat generation distribution depicted in figure 4.

The calculated values for the integrated ohmic and viscous heat generation in the fluid and the experimentally measured heat transfer to the walls of the accelerator are compared in figure 5 as functions of the Hartmann number. To give all the functions a zero value at $H = 0$, the calculated viscous heat generation for $H = 0$ was subtracted from all calculated values of viscous heating, and the measured heat-transfer values for $H = 0$ were subtracted from all measured values of heat transfer. As expected, the measured total heat transfer increases less rapidly with H than does the calculated total heat generation (solid curve), because some of the heat generated is not transferred to the walls but remains in the fluid. The apparent leveling off of the measured heat transfer at the larger Hartmann numbers is not understood; additional experimentation with stronger magnetic fields will be required to determine whether the apparent trend persists.

For nonzero values of the Hartmann number, the measured heat transfer to the upper electrode wall was consistently less than that to the lower electrode wall and, in some cases, was actually less than the heat transfer at

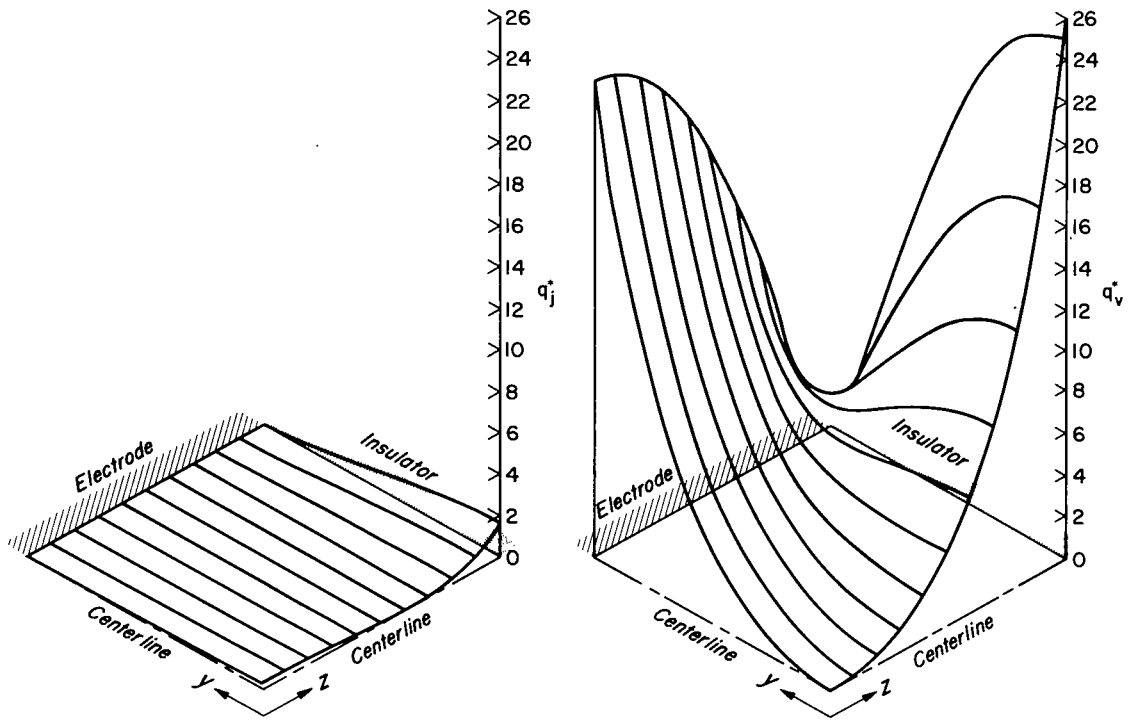

(a) Ohmic heat generation.

(b) Viscous heat generation.

Figure 3.- Heat generation for Hartmann number = 1.

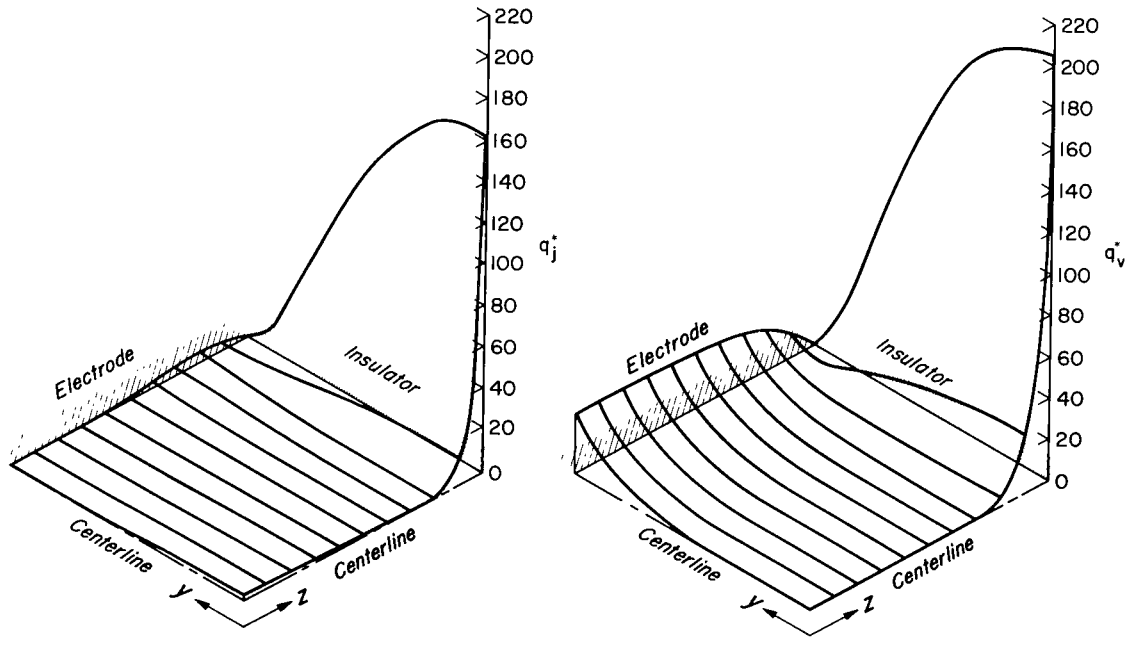

(a) Ohmic heat generation.

(b) Viscous heat generation.

Figure 4.- Heat generation for Hartmann number = 10.

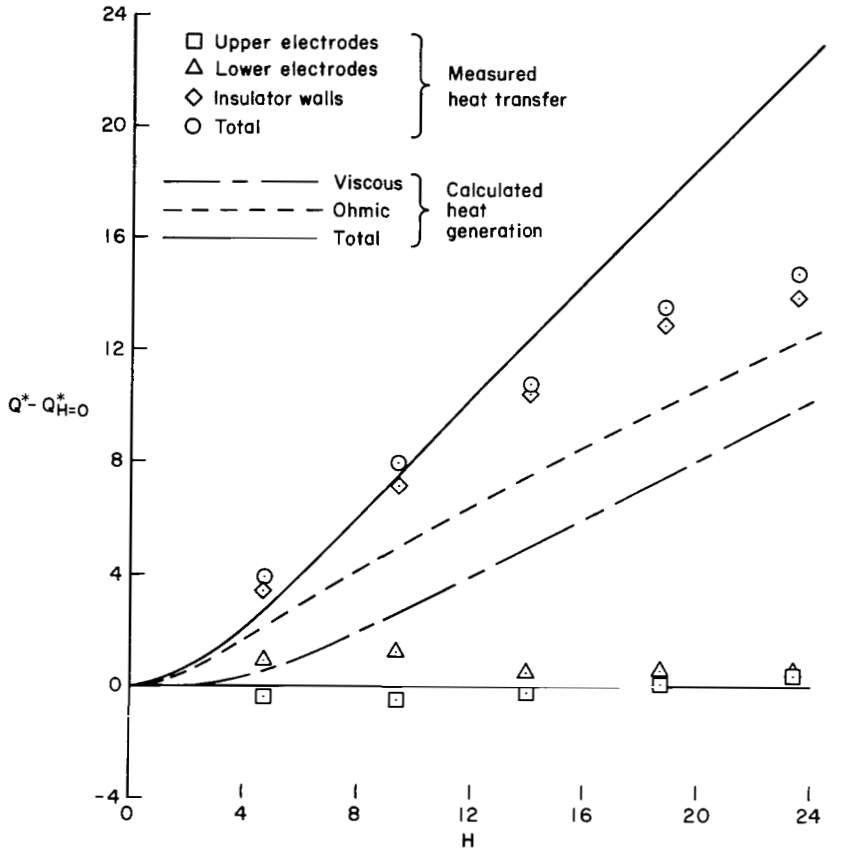

Figure 5.- Measured heat transfer and theoretical heat generation as a function of Hartmann number.

H = 0. This behavior is probably due to the Hall effect, which causes the circulating current density near the center of the duct (where j_y is negative) to have a component in the positive x direction. The resulting J × B force acts on the fluid in the negative y direction, tending to increase the pressure and the heat-transfer rate at the lower electrode wall.

The circulating currents work to decelerate the supersonic flow near the center of the duct by two mechanisms: enthalpy increase and J × B deceleration. For H = 10, the calculated value for j_y^* at y = z = 0 is -1.42, which, for the approximate operating conditions of the experiment corresponds to a current density of 5.74 A/cm^2. The one-dimensional theory of MHD duct flow predicts that a current density of this magnitude and a magnetic field of 0.214 tesla (H = 10) would result in a velocity decrease of 86 m/s for each centimeter of duct length. The measured and theoretical values of dynamic pressure at the stream centerline are shown in figure 6 as functions of the Hartmann number. The measured values were computed from the pitot probe data by means of the supersonic pitot tube formula, and the theoretical curve was calculated from equation (3) for y = z = 0. The theoretical decrease of dynamic pressure with increasing Hartmann number is in excellent agreement with the experimental measurements.

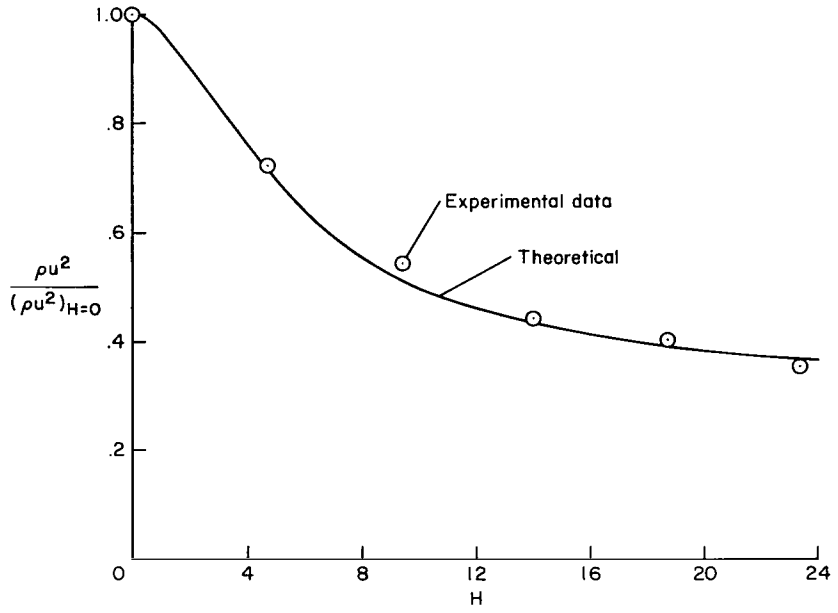

Figure 6.- Centerline dynamic pressure at the accelerator exit as a function of Hartmann number.

Both for the theory and for reducing the measured heat-transfer data to dimensionless form a spatially constant electrical conductivity was assumed. It is true that circulating currents would be impeded by a low conductivity near the insulator walls; however, the conductivity does not drop rapidly near the cold wall if the plasma has an elevated electron temperature. It was shown by Hale and Kerrebrock (ref. 18) that a two-temperature plasma flowing over a surface with a normal magnetic field results in a more uniform conductivity profile and much larger boundary-layer currents than does an equilibrium flow over the same surface. In some cases the conductivity profiles of Hale and Kerrebrock actually exhibit maximum peaks near the wall.

CONCLUDING REMARKS

The constant conductivity model of incompressible MHD duct flow predicts electrical currents circulating within the working fluid of an open circuit J × B device. These currents cause ohmic and viscous heat generation, which increase with magnetic field strength and are maximum near the insulator walls. Heat-transfer rates to the walls of an open circuit J × B plasma accelerator were measured; they increased with applied magnetic field strength at the insulator walls but remained nearly constant at the electrode walls. This distribution of heat transfer is qualitatively the same as the calculated heat generation distribution. The measured total heat-transfer rates are in good quantitative agreement with the calculated total heat generation rates. The magnitude and direction of the calculated circulating currents cause significant deceleration of the higher velocity flow near the center of the duct.

The problem of the circulating current will exist in any MHD duct in which there is an appreciable boundary layer and a large conductivity extending to near the walls.

Ames Research Center
National Aeronautics and Space Administration
Moffett Field, Calif. 94035, Feb. 17, 1969
129-02-08-01-00-21

REFERENCES

1. Kerrebrock, Jack L.: Electrode Boundary Layers in Direct-Current Plasma Accelerators. J. Aerospace Sci., vol. 28, no. 8, Aug. 1961, pp. 631-643.

2. Witalis, E. A.: Analysis of Linear MHD Power Generators. Plasma Physics (J. Nucl. Energy, pt. C), vol. 7, 1965, pp. 455-473.

3. Oliver, D. A.; and Mitchner, M.: Nonuniform Electrical Conduction in MHD Channels. AIAA J., vol. 5, no. 8, Aug. 1967, pp. 1424-1432.

4. Oliver, D. A.; and Mitchner, M.: Finite Ionization Rate Effects Over Electrodes in MHD Channels. AIAA J., vol. 6, no. 4, April 1968, pp. 732-734.

5. Argyropoulos, G. S.; Demetriades, S. T.; and Kendig, A. P.: Current Distribution in Nonequilibrium J × B Devices. J. Appl. Phys., vol. 38, no. 13., Dec. 1967, pp. 5233-5239.

6. Vedenov, A. A.: Round Table Discussion on Closed Cycle Systems. Electricity from MHD, Proc. Symposium on Magnetohydrodynamic Electrical Power Generation, International Atomic Energy Agency, Vienna, vol. 2, 1966, pp. 808-809.

7. Schneider, R. T.; and Wilhelm, H. E.: Experimental Investigation of Closed-Loop MPD Power Generation. Electricity From MHD, Proc. Symposium on Magnetohydrodynamic Electrical Power Generation, International Atomic Energy Agency, Vienna, vol. 2, 1966, pp. 551-566.

8. Reilly, J. P.; and Oates, G. C.: Insulator Boundary Layers in a Supersonic Magnetogasdynamic Channel. Paper 67-717, AIAA Electric Propulsion and Plasma Dynamics Conference (Colorado Springs, Colorado), Sept. 11-13, 1967.

9. Sutton, G. W.; and Sherman, A.: Engineering Magnetohydrodynamics. McGraw Hill, 1965, pp. 504-508.

10. Decher, R.; and Kerrebrock, J. L.: Electrode Wall-End Loop Shorting in a Nonequilibrium MHD Generator. Symposium on Engineering Aspects of Magnetohydrodynamics, 9th (University of Tennessee), April 3-5, 1968, pp. 142-155.

11. Shercliff, J. A.: Steady Motion of Conducting Fluids in Pipes Under Transverse Magnetic Fields. Proc. Cambridge Phil. Soc., vol. 49, pt. 1, Jan. 1953, pp. 136-144.

12. Hughes, W. F.; and Young, F. J.: The Electromagnetodynamics of Fluids. Wiley, 1966, pp. 195-215.

13. Stine, H. A.; Watson, V. R.; and Shepard, C. E.: Effect of Axial Flow on the Behavior of the Wall-Constricted Arc. AGARDograph no. 84, pt. 1, Sept. 1964, pp. 451-485.

14. Marvin, Joseph G.; and Deiwert, George S.: Convective Heat Transfer in Planetary Gases. NASA TR R-224, 1965.

15. Marvin, Joseph G.; and Akin, Clifford M.: Pressure and Convective Heat Transfer Measurements in a Shock Tunnel Using Several Test Gases. NASA TN D-3017, 1965.

16. Wald, David: Measuring Temperature in Strong Fields. Instruments and Control Systems, vol. 36, no. 5, May 1963, pp. 100-101.

17. De Voto, R. S.: Argon Plasma Transport Properties. Report SU-AA217, Institute for Plasma Research, Stanford Univ., 1965.

18. Hale, F. J.; and Kerrebrock, J. L.: Insulator Boundary Layers in Magnetohydrodynamic Channels. AIAA J., vol. 2, no. 3, March 1964, pp. 461-469.

NATIONAL AERONAUTICS AND SPACE ADMINISTRATION
WASHINGTON, D.C. 20546

OFFICIAL BUSINESS

FIRST CLASS MAIL

POSTAGE AND FEES PAID
NATIONAL AERONAUTICS AND
SPACE ADMINISTRATION

POSTMASTER: If Undeliverable (Section 158 Postal Manual) Do Not Return

"The aeronautical and space activities of the United States shall be conducted so as to contribute . . . to the expansion of human knowledge of phenomena in the atmosphere and space. The Administration shall provide for the widest practicable and appropriate dissemination of information concerning its activities and the results thereof."

—NATIONAL AERONAUTICS AND SPACE ACT OF 1958

NASA SCIENTIFIC AND TECHNICAL PUBLICATIONS

TECHNICAL REPORTS: Scientific and technical information considered important, complete, and a lasting contribution to existing knowledge.

TECHNICAL NOTES: Information less broad in scope but nevertheless of importance as a contribution to existing knowledge.

TECHNICAL MEMORANDUMS: Information receiving limited distribution because of preliminary data, security classification, or other reasons.

CONTRACTOR REPORTS: Scientific and technical information generated under a NASA contract or grant and considered an important contribution to existing knowledge.

TECHNICAL TRANSLATIONS: Information published in a foreign language considered to merit NASA distribution in English.

SPECIAL PUBLICATIONS: Information derived from or of value to NASA activities. Publications include conference proceedings, monographs, data compilations, handbooks, sourcebooks, and special bibliographies.

TECHNOLOGY UTILIZATION PUBLICATIONS: Information on technology used by NASA that may be of particular interest in commercial and other non-aerospace applications. Publications include Tech Briefs, Technology Utilization Reports and Notes, and Technology Surveys.

Details on the availability of these publications may be obtained from:

SCIENTIFIC AND TECHNICAL INFORMATION DIVISION

NATIONAL AERONAUTICS AND SPACE ADMINISTRATION

Washington, D.C. 20546